
Modeling the Vehicle-to-Vehicle (V2V) communication channel

Authors :

Alexis BOLLENGIER

Professor :

DE DONCKER Philippe

Academic year :

2024 - 2025

Contents

1	Introduction	1
2	Theoretical	2
2.1	Equivalent Circuit at TX and RX Terminals	2
2.2	Transverse Equivalent Heights of $\lambda/2$ Dipoles	2
2.3	Electric Field Emitted in Free Space	3
2.4	Relation V_{RX} as a Function of V_{TX}	3
3	LOS Channel	5
3.1	Channel Impulse Response $h(\tau)$ as a Function of d_1	5
3.2	Frequency Response of the Channel $H(f)$	5
3.3	Narrowband Transfer Function $h_{NB}(\tau)$	6
3.4	Received Power P_{RX} as a Function of Transmitted Power P_{TX}	6
3.4.1	Interpretation of Result	7
4	Full channel, narrowband analysis	8
4.1	Delays and Incidence Angles of Multipath Components	8
4.2	Received Power and Voltage for Each Reflection Order	9
4.3	Received Power P_{RX} vs. Transmit Power P_{TX} and Comparison to Friis' Formula	10
4.4	Estimation of the Rice K	11
4.5	Average Received Power in Local Areas and Path-Loss Model Fit	12
4.6	Variability Around the Path-Loss Model and Fade Margin	13
4.6.1	Fade Margin	14
4.6.2	Maximum Range	14
5	LOS channel, wideband analysis	16
5.1	Continuous-Time Impulse and Frequency Responses	16
5.2	Tapped-Delay-Line Impulse Response	16
6	Full channel, wideband analysis	18
6.1	Continuous-Time Impulse and Frequency Responses	18

6.2 Tapped-Delay-Line Model of the Full Channel 19

7 Further analyses: Doppler Effect and Power Delay Profile 20

1

Introduction

Vehicle-to-vehicle (V2V) communications form the basis of intelligent transportation systems by enabling the real-time exchange of safety and comfort data. Urban settings require an accurate channel model with complex building geometries and multiple propagation paths. This report presents a unified urban V2V model that uses a ray tracing method to capture the line of sight path and up to third-order multipath components.

We first review antenna representations, equivalent heights, and free-space radiation, then derive the narrowband LOS response. The model is then extended to third-order reflections to compute delays, received powers, the Rice factor, path-loss fitting and fading margin. Finally, the impulse response and a Tapped-Delay-Line representation is formulated for wideband analysis of only LOS and then extended to the full channel.

All simulations are conducted at a carrier frequency of $f_c = 5.9$ GHz with an RF bandwidth of $B_{RF} = 100$ MHz, employing vertical half-wave dipoles, a transmitted power $P_{TX} = 0.1$ W, and a receiver sensitivity of -70 dBm. The urban propagation environment is idealized as a 20-meter-wide street flanked by two rows of buildings with relative permittivity $\epsilon_r = 4$.

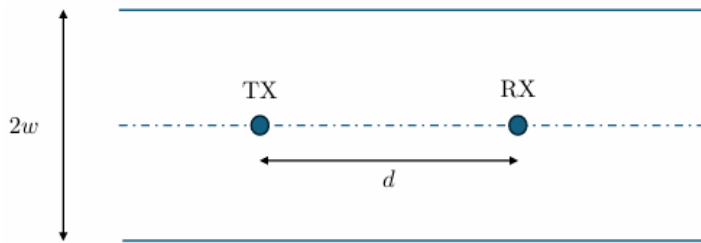
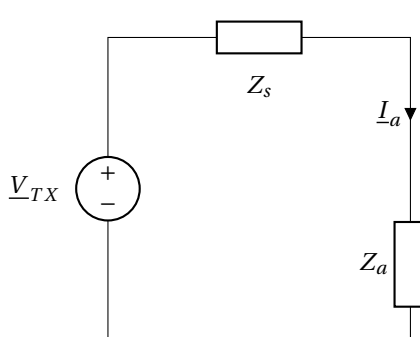


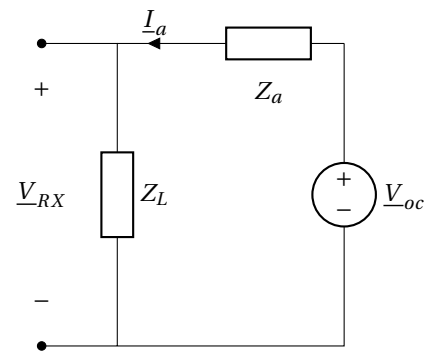
Figure 1.1: Geometry of the urban V2V link: street width $2w = 20m$, TX–RX separation $d < 1km$.

2.1 Equivalent Circuit at TX and RX Terminals

Figure (a) shows the transmit-side equivalent circuit: the generator voltage V_{TX} with internal impedance Z_S drives the antenna's input impedance Z_a and produces the antenna current I_a . Figure (b) depicts the receive-side model: the antenna appears as an open-circuit source V_{oc} in series with Z_a , feeding a load Z_L .



(a) Transmitter Circuit



(b) Receiver Circuit

2.2 Transverse Equivalent Heights of $\lambda/2$ Dipoles

For a vertical half-wave dipole antenna, the transverse equivalent height $h_{e\perp}$ characterizes the antenna's efficiency in transmission/reception.

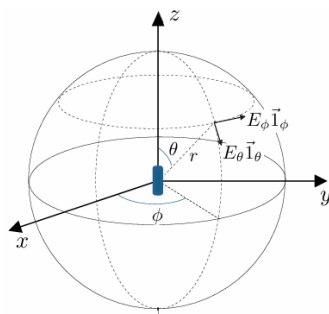


Figure 2.2: Electrical field radiated by an antenna located at the origin of the axes

According to the figure 2.2, its transverse component is given by:

$$\vec{h}_{e\perp}(\theta, \varphi) = -\frac{\lambda}{\pi} \frac{\cos\left(\frac{\pi}{2} \cos\theta\right)}{\sin\theta} \mathbf{1}_\theta$$

where $\mathbf{1}_\theta$ is a unit vector in the θ -direction. In the horizontal plane ($\theta = 90^\circ$), I have $\cos\left(\frac{\pi}{2} \cos 90^\circ\right) = \cos 0 = 1$ and $\sin 90^\circ = 1$. Thus, the transverse equivalent height reaches its maximum value in magnitude:

$$|\vec{h}_{e\perp}(90^\circ)| = \frac{\lambda}{\pi}$$

for each $\lambda/2$ dipole antenna (TX and RX) in the horizontal plane.

2.3 Electric Field Emitted in Free Space

In free space, the electric field radiated by the TX antenna decays as $\frac{1}{r}$ from the antenna. The general formulation of the emitted electrical field is given by:

$$\underline{\vec{E}}(\vec{r}) = -j\omega \underline{I}_a \frac{\mu_0}{4\pi} \frac{e^{-j\beta r}}{r} \vec{h}_{e\perp}(\theta, \varphi),$$

where $\beta = \frac{2\pi}{\lambda}$. Using the equivalent height of the $\lambda/2$ dipole obtained in 2.2, the classical expression for the far-field of a half-wave dipole is found. For a vertical dipole, the field is horizontal (direction $\mathbf{1}_\theta$) and is given by:

$$\underline{\vec{E}}_{hor}(r) = j \frac{Z_0 \underline{I}_a}{2\pi r} e^{-j\beta r} \mathbf{1}_\theta$$

where $Z_0 = \sqrt{\frac{\mu_0}{\epsilon_0}} = 377 \Omega$ is the free-space impedance. Replacing $r = c\tau$ (with c being the speed of light) and $\beta = \frac{2\pi f_c}{c}$, we obtain:

$$\underline{\vec{E}}_{hor}(r) = j \frac{Z_0 \underline{I}_a}{2\pi} \frac{e^{-j2\pi f_c \tau}}{c\tau} \mathbf{1}_\theta$$

Finally, expressing \underline{I}_a in terms of V_{TX} , we have $\underline{I}_a = \frac{V_{TX}}{Z_a + Z_s}$ for a perfectly matched antenna (with $Z_a = Z_s$). Then $\underline{I}_a = \frac{V_{TX}}{2Z_a}$. We can write the emitted field in terms of V_{TX} as:

$$\boxed{\underline{\vec{E}}_{hor}(r) = j \frac{Z_0}{4\pi Z_a} V_{TX} \frac{e^{-j2\pi f_c \tau}}{c\tau} \mathbf{1}_\theta}$$

2.4 Relation V_{RX} as a Function of V_{TX}

By combining the previous results, we can relate the received voltage V_{RX} to the transmitted voltage V_{TX} . The field emitted by the TX induces a voltage V_{oc} at the receiver given by $V_{oc}(\vec{r}) = -\vec{h}_{e\perp} \cdot \underline{\vec{E}}(\vec{r})$. In the horizontal plane, with $\vec{h}_{e\perp} = \frac{\lambda}{\pi} \mathbf{1}_\theta$ and $\underline{\vec{E}}_{hor}(r)$ from 2.3, we obtain :

$$V_{oc} = \frac{\lambda}{\pi} \underline{\vec{E}}_{hor}(r) = \frac{\lambda}{\pi} \left(j \frac{Z_0}{4\pi Z_a} V_{TX} \frac{e^{-j2\pi f_c \tau}}{c\tau} \right) = j \frac{Z_0 \lambda}{4\pi^2 Z_a} V_{TX} \frac{e^{-j2\pi f_c \tau}}{c\tau}.$$

For a matched receiver ($Z_L = Z_a$), the voltage across the load is half of V_{oc} (since the antenna impedance and the

load form an equal voltage divider):

$$\underline{V}_{RX} = \frac{1}{2} \underline{V}_{oc} = j \frac{Z_0 \lambda}{8\pi^2 Z_a} \underline{V}_{TX} \frac{e^{-j2\pi f_c \tau}}{c\tau}.$$

Replacing $\lambda = \frac{c}{f_c}$, we obtain:

$$\underline{V}_{RX}(\tau) = j \frac{Z_0}{8\pi^2 Z_a} \underline{V}_{TX} \frac{e^{-j2\pi f_c \tau}}{f_c \tau}$$

3

LOS Channel

3.1 Channel Impulse Response $h(\tau)$ as a Function of d_1

For a line-of-sight (LOS) channel, the impulse response is modeled as a single tap:

$$h(\tau) = \alpha_1 \delta(\tau - \tau_1)$$

where

$$\tau_1 = \frac{d_1}{c}$$

is the propagation delay (with c the speed of light). The complex amplitude α_1 is defined as:

$$\alpha_1 = a_1 e^{\phi_1} e^{-j2\pi f_c \frac{d_1}{c}},$$

where a_1 is the magnitude of the attenuation factor, ϕ_1 is the phase shift, and f_c is the carrier frequency. To highlight the $1/d_1$ dependence, we have factored the $1/d_1$ term out of the constant a_1 and grouped the remaining constant as $\zeta_1 = a_1 e^{\phi_1}$.

Note: For the rest of the report we rewrite $\zeta_1 = a_1 e^{\phi_1}$ for simplification.

The impulse response simplifies to:

$$h(\tau) = \frac{\zeta_1 e^{-j2\pi f_c \frac{d_1}{c}}}{d_1} \delta(\tau - \tau_1)$$

3.2 Frequency Response of the Channel $H(f)$

The frequency response $H(f)$ of the LOS channel is obtained by taking the Fourier transform of its impulse response:

$$H(f) = \int_{-\infty}^{\infty} h(\tau) e^{-j2\pi f \tau} d\tau$$

Since the delta function $\delta(\tau - \tau_1)$ selects the value at $\tau = \tau_1$, it follows that:

$$H(f) = \alpha_1 e^{-j2\pi f \tau_1} \quad (3.1)$$

Substituting the expression for α_1 from Section 3.1, we get:

$$H(f) = \frac{\zeta_1 e^{-j2\pi(f_c+f)\frac{d_1}{c}}}{d_1}$$

3.3 Narrowband Transfer Function $h_{NB}(\tau)$

Under the narrowband assumption, where the signal bandwidth is much smaller than the carrier frequency, the channel is considered frequency-flat. This means that the channel's response does not vary significantly across the signal's bandwidth.

The narrowband impulse response of the channel $h_{NB}(\tau)$ is, in the case of a single ray, simply equal to $h(\tau)$, and the signal received at the output of the channel $y(t)$ is given by:

$$y(t) = h_{NB}(t)x(t)$$

where:

$$h_{NB}(t) = h(t) = \alpha_1 \delta(t - \tau_1)$$

and $x(t)$ is the transmitted signal.

Thus, the narrowband impulse response $h_{NB}(\tau)$ is:

$$h_{NB}(\tau) = \frac{\zeta_1 e^{-j2\pi f_c \frac{d_1}{c}}}{d_1} \delta(\tau - \tau_1)$$

3.4 Received Power P_{RX} as a Function of Transmitted Power P_{TX}

When a signal scaled by V_{TX} is transmitted, the received voltage is

$$V_{RX} = V_{TX} h_{NB}(\tau) \quad \text{with} \quad h_{NB}(\tau) = h(\tau)$$

The received power is proportional to the square of the magnitude of the channel gain:

$$P_{RX} = P_{TX} \left| \frac{\zeta_1 e^{-j2\pi f_c \frac{d_1}{c}}}{d_1} \delta(\tau - \tau_1) \right|^2$$

Since the power of the complex exponential and the Dirac delta function is 1, the received power is simplified to

$$P_{RX} = P_{TX} \left(\frac{\zeta_1^2}{d_1^2} \right)$$

This expression shows that the received power decreases with the square of the distance d_1 , confirming the free space path loss.

The Friis formula for the received power P_{RX} is given by:

$$P_{RX}(d) = P_{TX} G_{TX} G_{RX} \left(\frac{\lambda}{4\pi d} \right)^2$$

where P_{TX} is the transmitted power and G_{TX} and G_{RX} are the gains of the transmit and receive antennas, respectively. The model obtained considers the power of the wave after passing through the antenna, not the initial transmitted signal, while the Friis formula also includes antenna gains and wavelength. By replacing the gain with $\frac{16}{3\pi}$ since the antennas are considered lossless dipoles.

$$\frac{P_{RX}}{P_{TX}} = G_{TX}G_{RX} \left(\frac{\lambda}{4\pi d_1} \right)^2$$

$$= \frac{16}{9\pi^2} \left(\frac{\lambda}{\pi d_1} \right)^2$$

It is possible to go from the formula obtained to the Friis formula by introducing the Poynting vector. Or also by equalizing the 2 formulas and see that we get:

$$\frac{\zeta_1^2}{d_1^2} = G_{TX}G_{RX} \left(\frac{\lambda}{4\pi d_1} \right)^2$$

$$\zeta_1 = \sqrt{G_{TX}G_{RX}} \cdot \frac{\lambda}{4\pi} = \frac{\lambda}{3\pi^2}$$

3.4.1 Interpretation of Result

The channel impulse response is modeled as a single tap with the delay $\tau_1 = \frac{d_1}{c}$. The absence of reflections means that the response depends only on the distance between the transmitter and receiver. The frequency response is a phase shift that varies with distance and carrier frequency, confirming that the LOS channel induces a frequency shift. Under the narrowband assumption, the channel is considered to be frequency flat, meaning that the response remains constant over the bandwidth of the signal and does not introduce frequency-dependent attenuation.

The received power decreases with the square of the distance d_1 , following the free space path loss model. The Friis formula includes antenna gain and wavelength and shows that as distance increases, received power decreases significantly. To compensate, one must either increase the transmit power or improve the antenna design. Doubling the distance requires quadrupling the transmit power, which is inefficient. The choice of wavelength affects both attenuation and data rate, with longer wavelengths reducing attenuation but limiting the maximum data rate due to the narrowband nature of the channel.

Full channel, narrowband analysis

4.1 Delays and Incidence Angles of Multipath Components

In this step we compute for each multipath component (MPC) up to third order, its one-way propagation delay τ and the angle of incidence θ at each reflection. We rely on the image-method of Ray Tracing.

- Computes the direct (LOS) path by measuring the straight-line distance between transmitter and receiver and converting it to delay via $\tau = \text{distance}/c$.
- For each single-bounce MPC, reflects the transmitter across each obstacle to get an “image” source, checks that the ray from that image to the receiver intersects the obstacle, and from the resulting impact point computes the total path length and corresponding delay, as well as the incidence angle at the bounce.
- Repeats this image-and-intersect procedure several times, depending on the reflection order, accumulating one delay value and one (or two, or three) incidence angles per path.

Results (Emitter at (10,10), Receiver at (110,10)):

Path Type	Delay τ (μs)	Incidence Angle(s) θ_i ($^\circ$)
Line-of-Sight (LOS)	0.333564	90.0000
Single reflection	0.340170	78.6901
Double reflection	0.359260	68.1986, 68.1986
Triple reflection	0.388999	59.0362, 59.0362, 59.0362

Table 4.1: Measured delays and all incidence angles for MPCs up to third order.

Since the reflecting walls are parallel, every reflected ray shares the same horizontal-to-vertical slope $\Delta x/\Delta y$, and therefore all incidence angles are identical:

$$\theta_i = 90^\circ - \arctan\left(\frac{\Delta y}{\Delta x}\right) = \arctan\left(\frac{\Delta x}{\Delta y}\right)$$

4.2 Received Power and Voltage for Each Reflection Order

We measure the received power P and voltage V (magnitude and phase) at the receiver for each propagation. With the formulas:

$$\Gamma_{\perp} = \frac{\cos \theta_i - \sqrt{\epsilon_r} \sqrt{1 - \epsilon_r^{-1} \sin^2 \theta_i}}{\cos \theta_i + \sqrt{\epsilon_r} \sqrt{1 - \epsilon_r^{-1} \sin^2 \theta_i}},$$

$$E_n(d) = \Gamma_{\perp} \sqrt{60 G_{\text{TX}} P_{\text{TX}}} \frac{e^{-j\beta d}}{d},$$

$$P_{\text{RX}} = \frac{1}{8 R_a^{\text{RX}}} \left| \sum_{n=1}^N \hat{\mathbf{h}}_{\perp}^{\text{RX}}(\theta_n, \phi_n) \cdot \mathbf{E}_n(\mathbf{r}) \right|^2.$$

with Γ_{\perp} : reflection coefficient, ϵ_r : permittivity of the buildings.

Note that for each reflection order two symmetric rays are contributing identical values, as you can see on 4.1

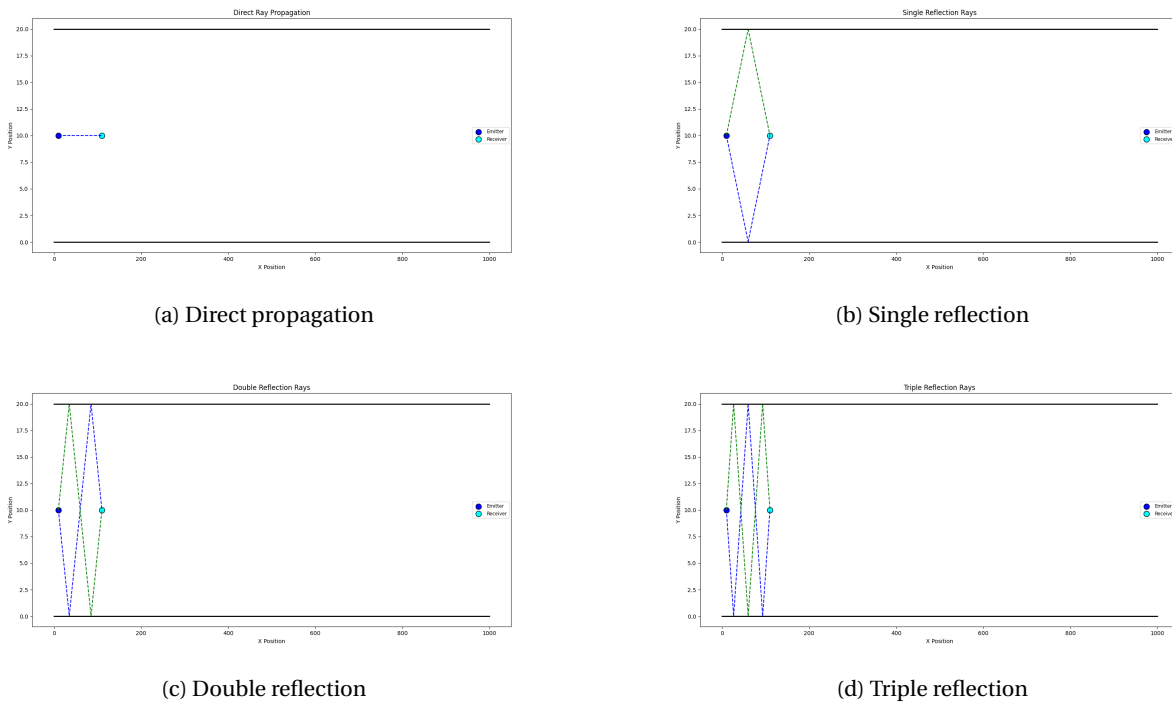


Figure 4.1: Ray-tracing diagrams for each propagation mechanism (emitter at (10,10), receiver at (110,10)).

Results (Emitter at (10,10), Receiver at (110,10)):

Path Type	P (W)	$ V $ (μ V)	$\angle V$ ($^{\circ}$)
LOS	4.56×10^{-10}	258.10	169.86
Single reflection (2 rays)	2.79×10^{-10}	201.90	-1.01
Double reflection (2 rays)	7.17×10^{-11}	102.30	-47.23
Triple reflection (2 rays)	9.99×10^{-12}	38.19	-34.38
Combined (all rays)	1.18×10^{-9}	384.27	-23.79

Table 4.2: Received power and voltage magnitude/phase for each reflection order and the combined total.

The LOS component remains the strongest contribution, while each higher-order reflection adds progressively

smaller power and voltage due to increased path length and reflection losses. Because the walls are parallel, each pair of symmetric reflections shares the same path length and phase. Their phasor sum therefore produces constructive and destructive interference, so the combined power and voltage diverge from the mere arithmetic sum of individual rays.

Results (Emitter at (10,13), Receiver at (110,9)):

Order	Ray	P (W)	$ V $ (μ V)	$\angle V$ ($^{\circ}$)
LOS	—	4.5554×10^{-10}	257.8943	-36.70
1 st reflection	Obstacle A	2.6531×10^{-10}	196.8117	-33.01
	Obstacle B	2.9377×10^{-10}	207.1001	123.81
2 nd reflection	A then B	6.0480×10^{-11}	93.9686	140.34
	B then A	8.5332×10^{-11}	111.6178	-62.04
3 rd reflection	A→B→A	9.0356×10^{-12}	36.3207	146.76
	B→A→B	1.1067×10^{-11}	40.1968	-34.21
Combined (all rays)		1.1805×10^{-9}	272.7155	-28.61

Table 4.3: Received power and voltage for each individual ray in the off-center scenario (Emitter at (10,13), Receiver at (110,9)).

In this off-center configuration, the two symmetric image-method rays at each reflection order traverse different path lengths, leading to distinct received powers and voltages for “left” versus “right” reflections. Only when the emitter and receiver lie exactly midway between the horizontal walls do these pairs coincide. The combined result again reflects phasor superposition, so its total power and voltage phase differ from the mere arithmetic sum of the individual rays.

4.3 Received Power P_{RX} vs. Transmit Power P_{TX} and Comparison to Friis' Formula

In Fig. 4.2a, the Friis model follows the expected d^{-2} slope, while the ray-tracing sum lies slightly above it because phase cancellation is ignored. Below ~ 100 m, the LOS ray alone dominates, explaining the close match between simulation and theory. Beyond a few meters, multipath components appear, and interference causes the received power to oscillate around the Friis curve (that computes only LOS power). The curve oscillates much less at larger separations and with only a few bounces, since the reflection angles change much less with distance.

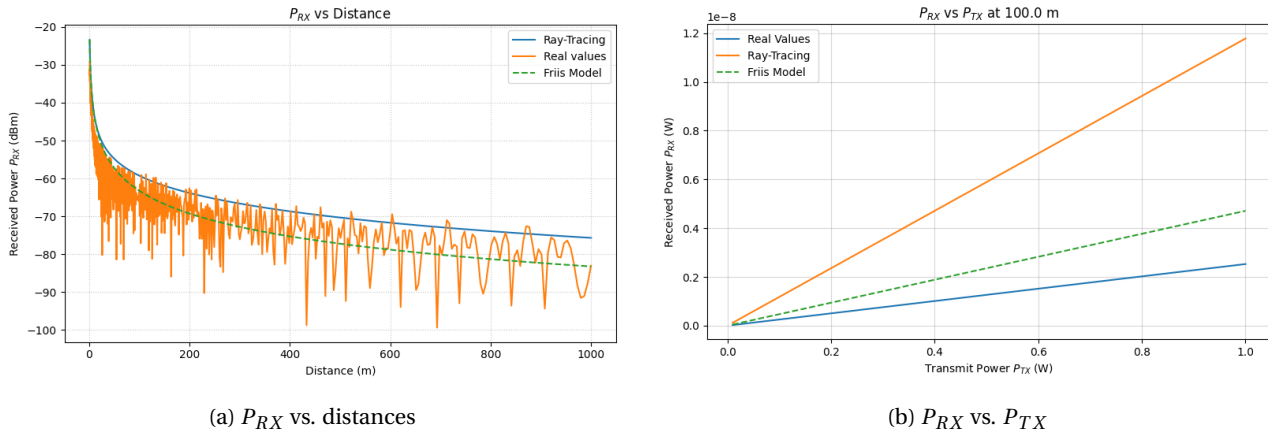


Figure 4.2: (a) Received power decay with distance. (b) Reference linear scaling of P_{RX} with P_{TX} .

4.4 Estimation of the Rice K

The Rice K -factor is defined as the ratio of the power of the LOS component to the power in all NLOS components. Equivalently, in terms of ray amplitudes a_n ,

$$K = \frac{a_0^2}{\sum_{n=1}^N a_n^2} \quad , \quad K_{\text{dB}} = 10 \log_{10} K$$

where a_0 is the amplitude of the LOS ray and a_n those of the N reflected rays.

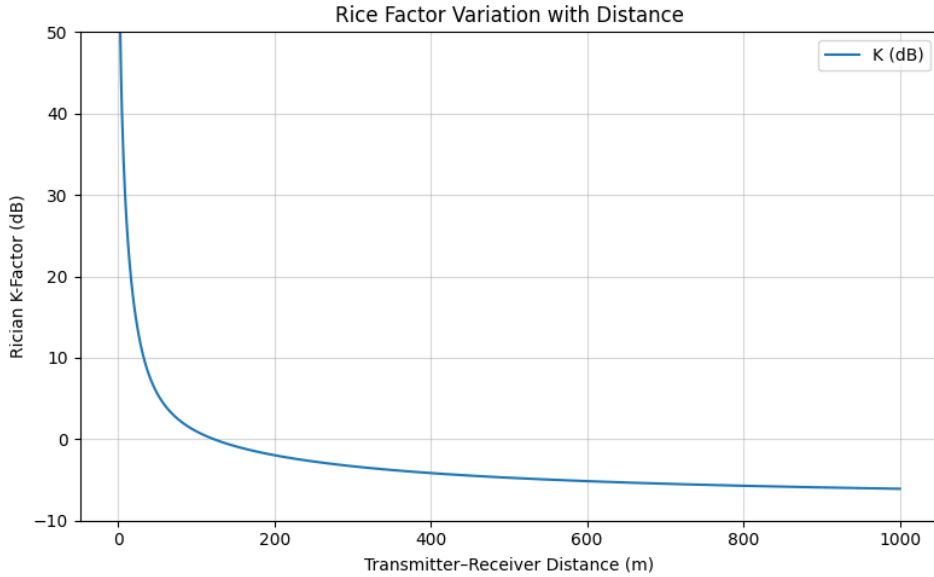


Figure 4.3: Rice K -factor (in dB) as a function of TX–RX distance

Figure 4.3 plots the Rice K -factor (in dB), which is computed from the ratio of the power in the LOS component to the sum of all reflected-path powers. Close to the transmitter, the LOS component is the only contributing and K_{dB} exceeds 40dB. As the distance increases, the relative power of the reflected paths grows, causing a rapid decrease in K_{dB} . Beyond a few hundred meters, K_{dB} approaches -5, dB, indicating that NLOS is dominating.

4.5 Average Received Power in Local Areas and Path-Loss Model Fit

The transmitter is at (500 m, 10 m). We split the 1 km street into $5 \text{ m} \times 5 \text{ m}$ cells and compute each cell's average received power via

$$V_{\text{oc}}(\mathbf{r}) = -\hat{\mathbf{h}}_{\perp}^{\text{RX}}(\theta_n, \phi_n) \mathbf{E}_n(\mathbf{r}),$$

$$\langle P_{\text{RX}} \rangle = \frac{1}{8 Z_a} \sum_{n=1}^N |V_{\text{oc},n}|^2$$

where

- $\langle P_{\text{RX}} \rangle$ is the average power in one cell,
- Z_a is the antenna impedance,
- $V_{\text{OC},i}$ is the open-circuit voltage induced by ray i ,
- N is the number of rays within that cell.

Convert to dBm by

$$\bar{P}_{\text{RX}}(x, y) = 10 \log_{10}(\langle P_{\text{RX}}(x, y) \rangle / 10^{-3}) \text{ dBm}.$$

Figures 4.4 show the spatial distribution of \bar{P}_{RX} for different resolutions.

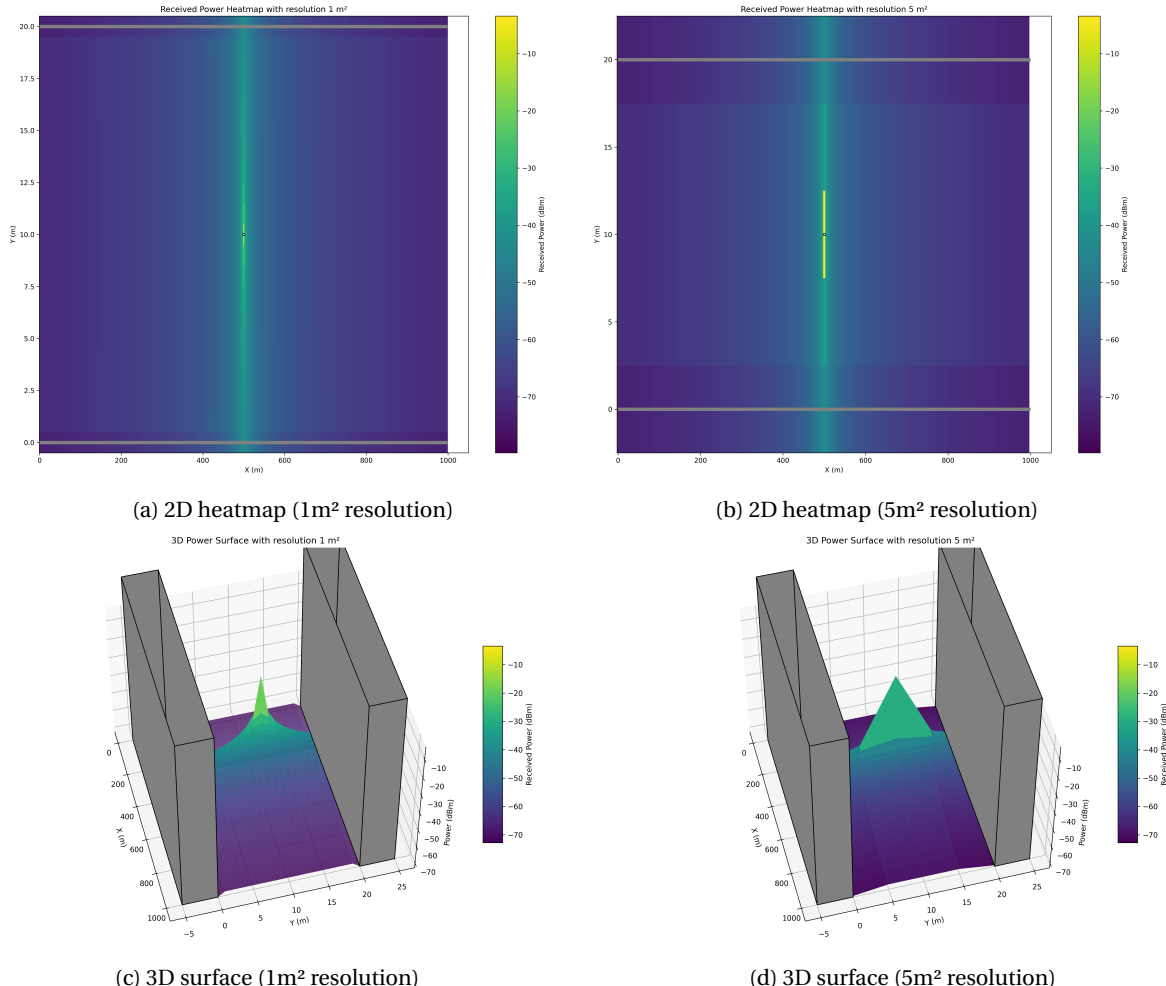


Figure 4.4: Received power distribution at two spatial resolutions

We define the path loss for 1D and 2D cases. Indeed with 1D the receiver moving along the centerline and in 2D by taking into account all the position on the road, at each distance d_i we define path loss

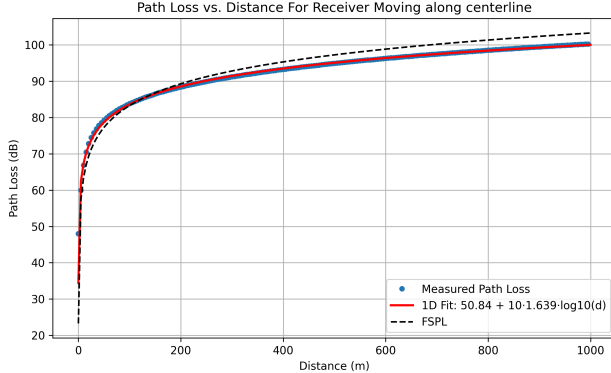
$$L_0(d_i) = P_{\text{TX}} - \bar{P}_{\text{RX}}(d_i) + 20 \log_{10} G_{\text{TX}}.$$

To model the distance dependence, we fit the log-distance

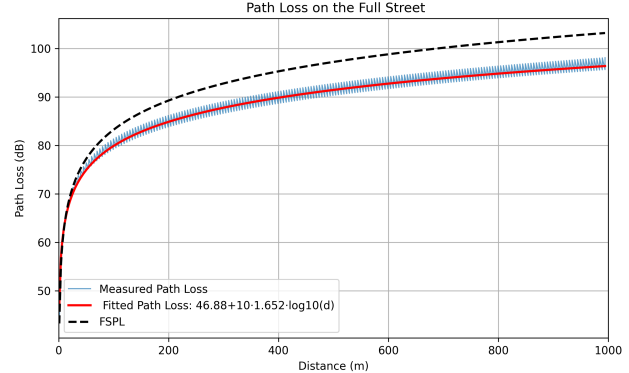
$$L_0(d) = L_0(d_0) + 10 n \log_{10}(d/d_0), \quad d_0 = 1 \text{ m.}$$

We perform a linear regression of $L(d_i)$ versus $\log_{10}(d_i)$ using the least squares method, which returns the intercept $L_0(d_0)$, the slope $10 n$, and the coefficient of determination R^2 . The regression yields

$$\begin{aligned} \text{centerline : } & L_0(d_0) = 50.84 \text{ dB}, \quad n = 1.639, \quad R^2 = 0.998, \\ \text{full street: } & L_0(d_0) = 46.88 \text{ dB}, \quad n = 1.652, \quad R^2 = 0.973. \end{aligned}$$



(a) Path loss vs. distance along the centerline.



(b) Path loss vs. distance along the full street .

Figure 4.5: Measured Path Loss, fitted log-distance model, and Friis Path Loss.

For further, we decide to keep the Path loss across the full street, as in real life, cars are most of the time not in the same line. Figure 4.5 shows that summing individual path powers yields a path-loss exponent $n = 1.652$, below the free-space exponent($n=2$), because reflected rays contribute only in additional power. The high R^2 confirms the quality of the linear fit in the log-distance domain.

4.6 Variability Around the Path-Loss Model and Fade Margin

We evaluated the measured path loss around the fitted log distance law by computing residuals for the full-street path loss.

$$\Delta_i = L(d_i) - [L_0(d_0) + 10 n \log_{10}(d_i/d_0)],$$

whose standard deviation is¹

$$\sigma_L = \sqrt{\frac{1}{N-1} \sum_{i=1}^N (\Delta_i - \bar{\Delta})^2} = 1.18 \text{ dB.}$$

¹We got $\sigma_L = 0.52$ dB for the Path Loss along the centerline street

This unusually low deviation arises from our simplifying assumptions, such as limiting to three reflections and neglecting diffraction and other scattering, which reduce the variability compared to channels in the real world.

4.6.1 Fade Margin

The link success probability for a fade margin M is

$$\Pr(\Delta > M) = \frac{1}{2} \operatorname{erfc}\left(\frac{M}{\sigma_L \sqrt{2}}\right).$$

$$1 - \Pr(\Delta < M) = \frac{1}{2} \operatorname{erfc}\left(\frac{M}{\sigma_L \sqrt{2}}\right).$$

To achieve reliability p , the required margin is

$$M(p) = \sigma_L \sqrt{2} \operatorname{erfcinv}[2(1 - p)],$$

giving numerically

$$M(50\%) = 0.000 \text{ dB},$$

$$M(95\%) = 1.938 \text{ dB},$$

$$M(99\%) = 2.741 \text{ dB}.$$

4.6.2 Maximum Range

Including the fade margin in the link budget,

$$P_{\text{TX}} - P_{\text{sens}} - M(p) + 20 \log_{10} G_{\text{TX}} = L_0(d_0) + 10 n \log_{10}(d_{\max}/d_0),$$

yields

$$d_{\max} = d_0 10^{\frac{P_{\text{TX}} - P_{\text{sens}} - M(p) + 20 \log_{10} G_{\text{TX}} - L_0(d_0)}{10 n}}.$$

With

$$d_0 = 1 \text{ m}, P_{\text{TX}} = 20 \text{ dBm}, P_{\text{sens}} = -70 \text{ dBm}, G_{\text{TX}} = 1.7, L_0(d_0) = 46.88 \text{ dB}, n = 1.652,$$

We find the following maximum ranges:

Reliability p	Fade Margin M [dB]	d_{\max} [m]
50%	0.000	773.171
95%	1.938	590.159
99%	2.741	527.676

Table 4.4: Required fade margin and resulting maximum range across the full street.

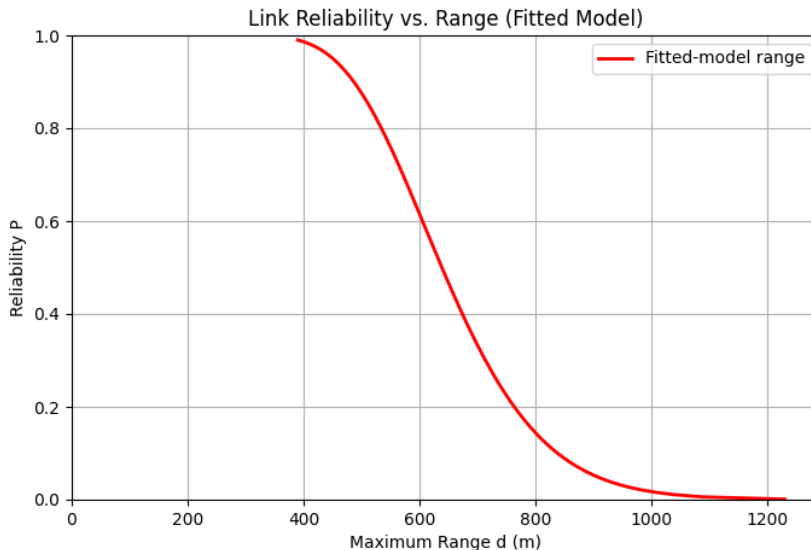


Figure 4.6: Link reliability versus maximum range for the full street

It is also interesting to compare it with the centerline fit model:

Reliability p	Fade Margin M [dB]	d_{\max} [m]
50%	0.000	467.205
95%	0.449	438.670
99%	0.635	427.364

Table 4.5: Required fade margin and resulting maximum range for the centerline

By comparing Tables 4.4 and 4.5, the full street model consistently predicts higher values d_{\max} because it incorporates lateral reflections and spatial averaging throughout the roadway, while the centerline transect considers only on-axis measurements and therefore underestimates power.

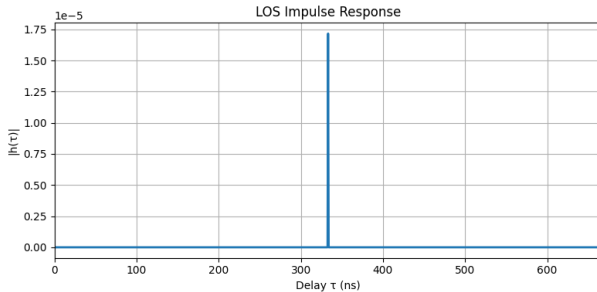
LOS channel, wideband analysis

5.1 Continuous-Time Impulse and Frequency Responses

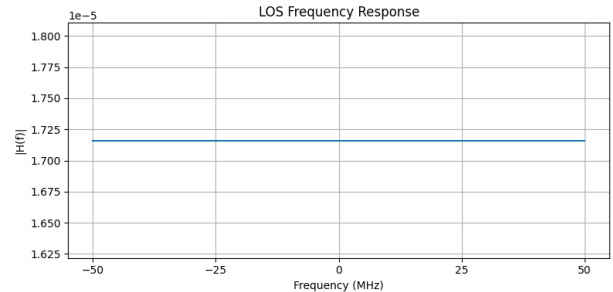
Starting from the single-ray LOS model, the impulse response is the same as in 3.1

$$h(\tau) = \frac{\zeta_1 e^{-j2\pi f_c \tau_1}}{d_1} \delta(\tau - \tau_1)$$

The frequency response of the channel has been found by taking its Fourier transform, as shown in equation 3.1. The channel has a bandwidth of 100 MHz, which leads to a frequency response magnitude limited to ± 50 MHz around the carrier frequency. 5.1b shows the response in baseband.



(a) Impulse-response magnitude $|h(\tau)|$



(b) Frequency-response magnitude $|H(f)|$

Figure 5.1: LOS wideband channel Impulse Response for TX-RX of 100m

5.2 Tapped-Delay-Line Impulse Response

A receiver with finite RF bandwidth B_{RF} cannot distinguish multipath components arriving within less than

$$\Delta\tau = \frac{1}{B_{RF}}.$$

Thus, the continuous impulse response $h(\tau) = \sum_{n=1}^N \alpha_n \delta(\tau - \tau_n)$ is effectively sampled by a series of taps spaced by $\Delta\tau$. From wideband channel theory, each tap coefficient is obtained by filtering the true response with a sinc of width B_{RF} :

$$h_l = \int_0^\infty h(\tau) \operatorname{sinc}[B_{RF}(\tau - l\Delta\tau)] d\tau.$$

For the single-ray LOS case $h(\tau) = \alpha_1 \delta(\tau - \tau_1)$, this simplifies to

$$h_l = \alpha_1 \operatorname{sinc}[B_{\text{RF}}(\tau_1 - l \Delta \tau)], \quad \alpha_1 = \frac{\zeta_1 e^{-j2\pi f_c \tau_1}}{d_1},$$

Therefore the TDL model becomes

$$h_{\text{TDL}}(\tau) = \sum_{l=0}^L \frac{\zeta_1 e^{-j2\pi f_c \tau_1}}{d_1} \operatorname{sinc}[B_{\text{RF}}(\tau_1 - l \Delta \tau)] \delta(\tau - l \Delta \tau).$$

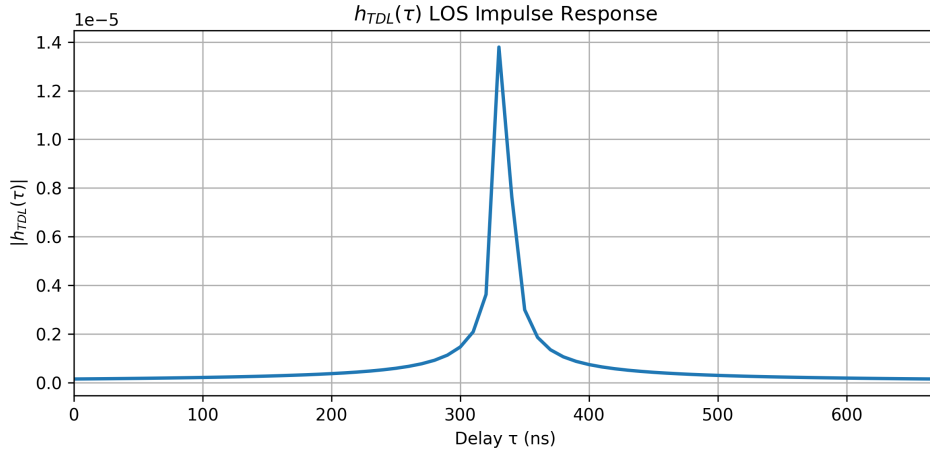


Figure 5.2: TDL Impulse Response for TX-RX of 100m

Restricting the RF bandwidth to B_{RF} “smears” the ideal delta at τ_1 into a sinc-shaped pulse, lowering the main-lobe peak below ζ_1/d_1 and distributing energy into sidelobes. Truncating the taps to $L+1$ bins encompassing the channel’s maximum delay spread discards any remaining sidelobe energy, so the outermost taps have near-zero amplitude. We adopt the TDL representation because it matches the physical limits of real receivers (finite bandwidth and delay resolution).

6

Full channel, wideband analysis

6.1 Continuous-Time Impulse and Frequency Responses

The received baseband signal is the superposition of N delayed and attenuated replicas of the transmit waveform. Injecting an impulse $x(t) = \delta(t)$ yields the channel impulse response

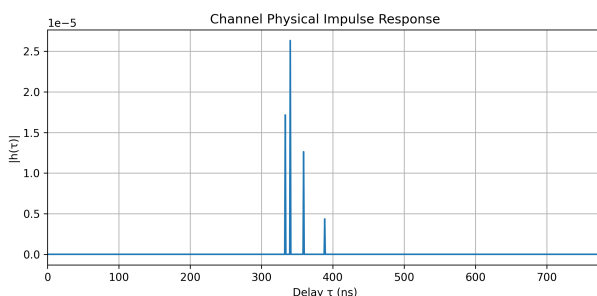
$$h(\tau) = \sum_{n=1}^N \alpha_n \delta(\tau - \tau_n),$$

where each complex gain $\alpha_n = a_n e^{j\phi_n} e^{-j2\pi f_c \tau_n}$ combines amplitude a_n , non-propagation phase ϕ_n , and propagation phase $-2\pi f_c \tau_n$, and τ_n is the path delay.

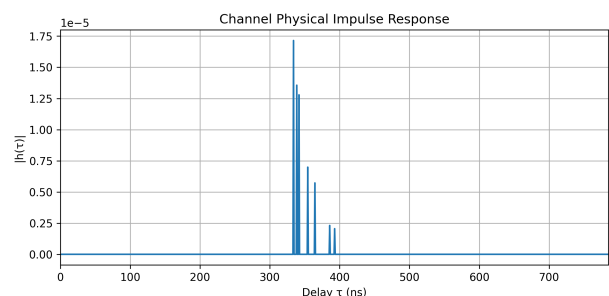
Scenario Definitions It has been decided to analyze two different configurations of transmitter and receiver positions:

1. **Scenario 1:** Transmitter at (10, 10), Receiver at (10, 110).
2. **Scenario 2:** Transmitter at (13, 10), Receiver at (9, 110).

Figure 6.1a shows the impulse response $|h(\tau)|$ for TX and RX aligned laterally. Although seven physical rays exist, only four delay taps appear because parallel walls produce equal-length path pairs that merge into the same delay bin. In contrast, Figure 6.1b corresponds to a scenario with TX and RX at different x and y positions, breaking the symmetry and yielding seven distinct delay taps, one for each ray.



(a) Scenario 1 full-channel impulse-response



(b) Scenario 2 full-channel impulse-response

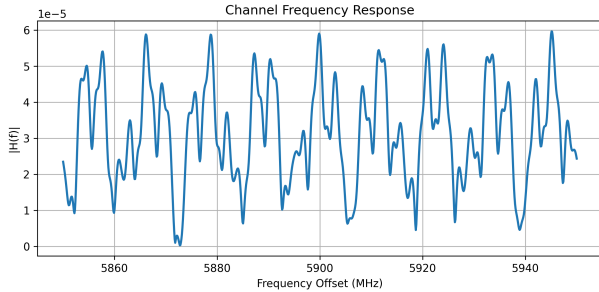
Figure 6.1: Comparison of two impulse-response plots combining LOS and multipath up to third order.

Physically, each delta pulse represents one propagation path. Its amplitude decays with distance and reflection

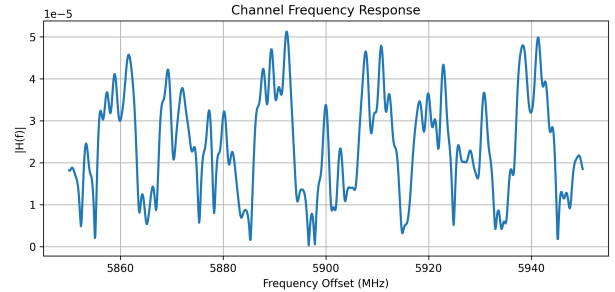
losses. The total delay span the channel's maximum delay spread determines the coherence bandwidth and the degree of frequency selectivity.

Figure 6.2 shows the full-channel amplitude spectrum around the 5.9 GHz band. Because each reflected path arrives with a different delay and attenuation, the total response exhibits rapid peaks and dips as frequency varies.

In particular, Figure 6.2a confirms that $f_c = 5.9$ GHz is at a maximum of $|H(f)|$, making it an excellent operating point for this geometry. By contrast, Figure 6.2b demonstrates that a small shift to around 5.886 GHz would yield even higher gain, while slightly higher or lower offsets suffer deeper fades. This sensitivity shows that, in a multipath environment, the “best” carrier frequency can change rapidly.



(a) Scenario 1 Frequency-response

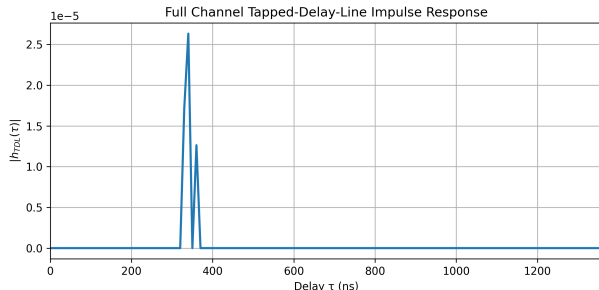


(b) Scenario 2 Frequency-response

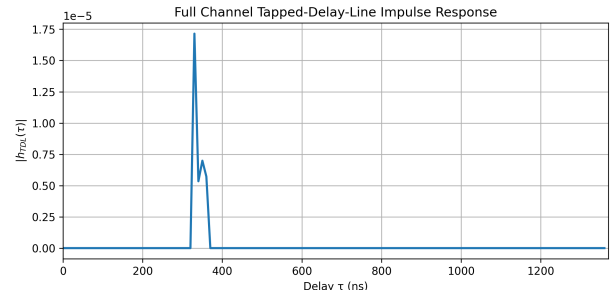
Figure 6.2: Full-channel frequency-response

6.2 Tapped-Delay-Line Model of the Full Channel

With the same explanation given in 5.2. The TDL impulse Response for the 2 scenarios are shown below



(a) TDL Impulse Response Scenario 1



(b) TDL Impulse Response Scenario 2

Figure 6.3: TDL Impulse Response for the full channel.

In Figure 6.3(a), the transmitter and receiver share the same lateral coordinate, so symmetric reflection paths collapse into identical delays and yield to a peak with a bigger amplitude and a visible sidelobe due to a little delay, probably due to the 3 reflections path. In contrast, when Tx and Rx are different in both x and y Fig. 6.3(b), each of the seven physical rays arrives at a distinct delay, creating a larger peak. In both cases, the channel's delay spread is increased, thereby reducing its coherence bandwidth. The delayed taps overlap neighbouring symbols and may cause ISI whenever this spread exceeds the symbol interval.

Further analyses: Doppler Effect and Power Delay Profile

In Scenario 2, we introduce vehicle motion at

$$v = 50 \text{ km/h} \approx 13.89 \text{ m/s} \quad \text{with} \quad f_c = 5.9 \text{ GHz.}$$

Since $\lambda = c/f_c$, the maximum Doppler shift is

$$f_{D,\max} = \frac{v}{\lambda} = \frac{v f_c}{c} \approx 273 \text{ Hz.}$$

Each multipath ray arriving at angle θ_i yields

$$f_{D,i} = \frac{v}{\lambda} \cos \theta_i,$$

and from the collection $\{f_{D,i}\}$ we obtain the empirical Doppler spectrum:

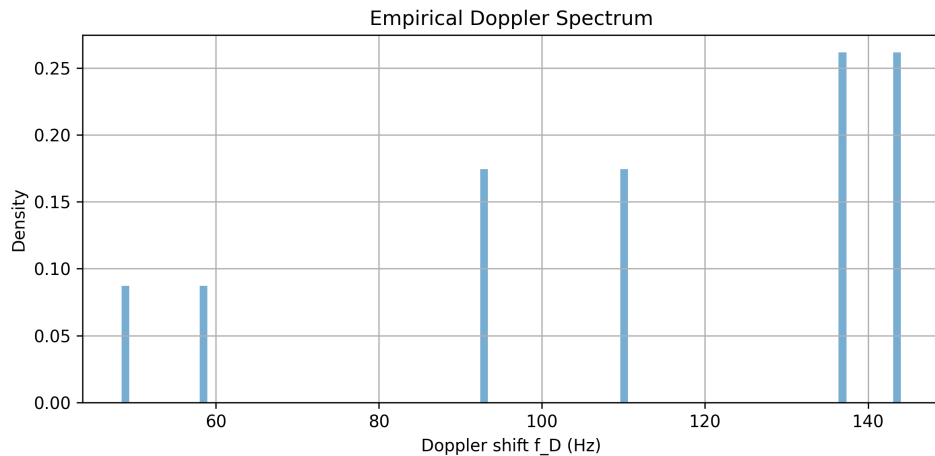


Figure 7.1: Empirical Doppler spectrum $P_{\text{emp}}(f_D)$.

Each distinct peak corresponds to one propagation path in our finite-ray model. From $f_{D,\max}$ the channel coherence time follows the classical Clarke approximation:

$$T_c \approx \frac{\lambda}{2v} = \frac{c}{2v f_c} \approx 1.83 \text{ ms},$$

If $T_s \ll T_c$, the channel varies slowly over a symbol interval (slow fading), so amplitude and phase remain approximately constant and can be tracked easily. If $T_s \gtrsim T_c$, the channel changes appreciably within one symbol (fast fading).

ing), leading to rapid amplitude fluctuations. If fast fading occurs, more complex solutions are required to maintain reliable communication.

Given a normalized Power Delay Profile with taps $\{(\tau_\ell, P_\ell)\}$ satisfying $\sum_\ell P_\ell = 1$, we compute

$$\bar{\tau} = \sum_\ell \tau_\ell P_\ell, \quad \sigma_\tau = \sqrt{\sum_\ell (\tau_\ell - \bar{\tau})^2 P_\ell}.$$

In our implementation $P_\ell = |a_\ell|^2 / \sum_k |a_k|^2$, yielding

$$\bar{\tau} \approx 358.76 \text{ ns}, \quad \sigma_\tau \approx 21.44 \text{ ns}.$$

Since $B_c \approx 1/(2\pi\sigma_\tau) \approx 7.42$ MHz is much smaller than $B_{RF} = 100$ MHz, the channel remains strongly frequency-selective as discussed in 6.2

Pilot tones are known reference symbols inserted at regular intervals in time and frequency to enable the receiver to estimate and track the channel's amplitude and phase. Because $T_c \approx 1.83$ ms, time-domain pilots only need to appear every few symbols. In frequency, since $B_c \approx 7.42$ MHz, pilot subcarriers must be spaced well below 7 MHz to sample the fades without aliasing. Finally, the mean delay plus several RMS spreads is ≈ 359 ns, so with a sampling rate of 20 MHz (50 ns per tap) an equalizer requires at least 6–8 taps to cover the delay spread. Modulation and coding should exploit the channel's quasi-static behavior within each coherence block.